Science and Technology Indonesia
e-ISSN:2580-4391 p-ISSN:2580-4405
Vol. 8, No. 4, October 2023

Research Paper

# Studying the Structure Properties of Copper Nanoparticles Prepared by Chemical Reduction Method

Noora H. Al-Zobiadi[1*], Ammar A. Habeeb[2], Awatif S. Jasim[1]

[1]*Department of Physics, College of Science, Tikrit University, Tikrit, 34001, Iraq*
[2]*Department of Physics Science, University of Diyala, 34005, Iraq*
***Corresponding author**: noora.h.shallal.phys505@st.tu.edu.iq*

**Abstract**
The chemical reduction method (CRM) can produce high purity nanoparticles, it is a down-top chemical method based on the principle of salt reduction, this method is used in this work to synthesis copper nanoparticals (CuPNs) by use different concentrations of copper nitrate. The properties of the prepared nanoparticles were studied by fourier transform infrared (FTIR) and ultraviolet-visible (UV-Vis) spectroscopy were used to measure the absorbance spectra of the produced particles. According to the scanning electron microscope (SEM), the particles' diameters range from (61.64 to 49.25) nm. According to X-ray diffraction, the particles exhibit a face monoclinic crystal structure (FCC). According to the transmission electron microscope findings, the particles are asymmetrically spherical in shape.

**Keywords**
Chemical Reduction, Copper, (UV-Vis) Spectroscopy, FTIR, TEM

Received: 11 June 2023, Accepted: 7 August 2023
https://doi.org/10.26554/sti.2023.8.4.640-646

## 1. INTRODUCTION

Due to their high surface-to-volume ratio, nanoparticles (NPs) exhibit favorable and uncommon physical and chemical characteristics, as well as favorable biological activities (Majumdar et al., 2019; Huang et al., 2017; He et al., 2019). Copper is a heavy metal Johnson et al. (2011) and metal oxides affect the environment in both beneficial and harmful ways (Hawthorne et al., 2012; Johnson et al., 2011; Zhou et al., 2006). In the sphere of technological applications, copper nanoparticles are used as catalysts, magnetic storage devices, batteries, solar cells, and gaseous excited (Xu et al., 2009; Zhi Ang et al., 2009; Wu et al., 2010; Nakamura et al., 2019).

There are several physical methods that can be used to create copper nanoparticles, including pulsed laser ablation in liquid Vinod and Gopchandran (2014) and chemical methods such as reduction (Seo et al., 2018; Jardón-Maximino et al., 2021) and chemical degradation (Brycki et al., 2020). Chemical reduction is a cheap and easy method that allows the formation of nanoparticles and can reduce their size (Harada et al., 2020; Karthik and Singh, 2015) such as sodium borohydride or hydrazine, to create smaller nanoparticles or to reduce reduction time (Zahoor et al., 2021). Both silver and gold are utilized to create nanoparticles from noble metals (Benassai et al., 2021; Nagar and Devra, 2018) and because it is less expensive and has particles with a diameter of around 25 nm, copper is utilized in place of these materials Duan et al., 2015; Khalid et al., 2016).

In this study, copper nanoparticles were synthesized by the chemical precipitation method, and their structural properties and concentration were known first, the CuO nanoparticles were prepared by the chemical reduction method and different from studies (Alzahrani, 2018; Jayaramudu et al., 2019) second, and all of the products are in the film form. All films are prepared by the drop-casting method. The characterization of this film with (UV-Vis), (AAS), (FTIR), (SEM), (XRD) and (TEM).

## 2. EXPERIMENTAL SECTION

### 2.1 Material

$Cu(NO_3)_2.3H_2O$ and Deionized water were the materials employed in this study. Sodium Borohydride ($NaBH_4$), and pure ethanol ($CH_2CH_3OH$). Table (1) displays the characteristics of the materials employed in this study.

At room temperature and in the dark, aqueous copper nitrate was dissolved in a solution of deionized water and absolute ethanol in a 1:1 ratio using different molar concentrations (0.24, 1.2, and 2.4) mM of each substance. The solution was then put on the magnetic mixer. Since the preparation process took

**Table 1.** Materials Used in The Study

| Raw Material | Chemical Formula | Molecular Weight | Physical Characteristics | Manufacturer |
|---|---|---|---|---|
| Copper Nitrate | $Cu(NO_3)_2.3H_2O$ | 241.6 | Blue | Himdia |
| Sodium Borohydride | $NaBH_4$ | 37.83 | White | Avonchem |
| Ethanol Absolute | $CH_2CH_3OH$ | 46.07 | Colorless | Hayman Group Ltd. – UK |

**Table 2.** Values of Concentration Copper Nanoparticles

| M (mM) | Cu Ppm |
|---|---|
| 0.24 | 131.6024 |
| 1.2 | 161.0227 |
| 2.4 | 294.5873 |

**Figure 1.** Copper Nanoparticle Solution

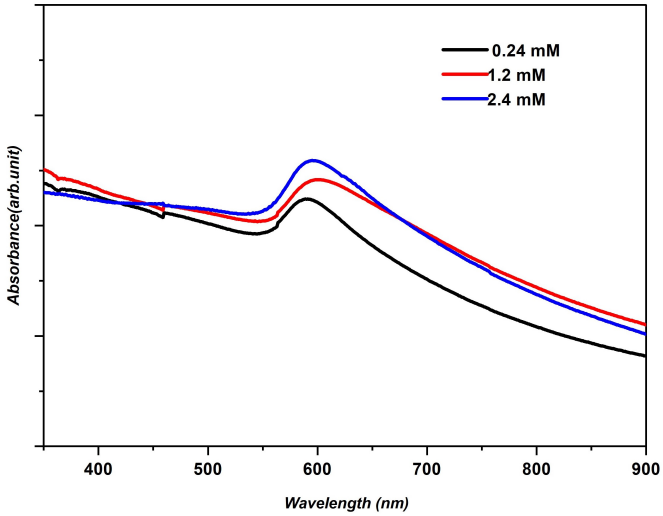


**Figure 2.** Absorption Spectrum of Copper Nanoparticles

three hours and the amount added was roughly (200 µL), a solution of the reducing agent with a concentration of (26.2 µM) was gradually added to the solution while it was being continuously stirred. This was done until the color of the solution changed from light blue to light gray-green, the color change indicates the formation of nanoparticles (Rashid et al., 2022). The solution record is depicted in the following Figure (1).

## 3. RESULTS AND DISCUSSION

### 3.1 UV-Visible Spectroscopy of Copper Nanoparticles (UV-VIS)

The produced solution with various molar concentrations was examined by ultraviolet-visible absorption, which is an efficient approach to determining the shape and size of nanoparticles. Figure (2) demonstrates how the concentration of the produced nanoparticles increased together with the molar concentration of the CuNPs solution, changing the hue of the solution The figure above depicts the variation in the CuNPs solution's absorption spectra as a function of wavelength and the appearance of copper nanoparticle surface plasmon resonance (SPR) peaks at wavelengths (587, 591, and 595) nm agrees with the study Patil et al. (2018) which correspond to molar concentrations (0.24, 1.2, and 2.4) mM, respectively. The small average size of the generated nanoparticles with an increase in the molar concentrations utilized in the preparation procedure is thought to be the cause of the emergence of these peaks. The reason for the appearance of peaks indicates the formation of nanoparticles, and an increase in the absorbance values means an increase in the production of nanoparticles, the absorbance values are (0.22, 0.27, and 0.28), resulting in (Gondal et al., 2013). These peaks support the presence of NPs in the solution and show that the surface plasmon resonance (SPR) peak shifted toward shorter wavelengths (blue shift) as concentration increased.

### 3.2 Atomic Absorption Spectroscopy (AAS)

An atomic absorption spectrometer was used to analyze the concentrations of copper nanoparticles, and the results revealed that the concentrations of the particles varied. It was determined that the prepared particle concentration increased with increasing molar concentrations. Copper nanoparticle concentration results are displayed in Table (2).

### 3.3 FTIR Results of Copper Nanoparticles

Figure (3) shows a spectrum (FTIR) of copper nanoparticles after being prepared by the chemical precipitation method and at different molar concentrations (0.24, 1.2, 2.4)mM. Three

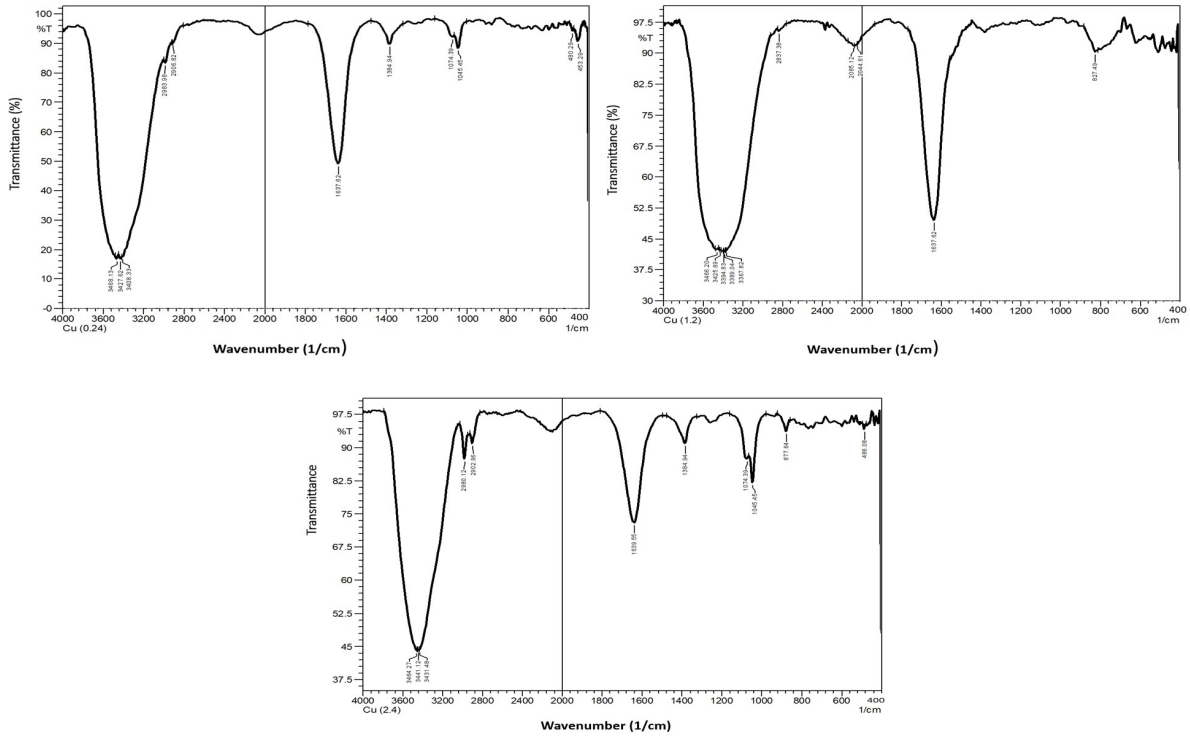


**Figure 3.** FTIR of Copper Nanoparticles

**Table 3.** Structural Properties of Copper Nanoparticles

| M (mM) | Geometric Crystal System | 2$\theta$ (deg) | hkl | FWHM (deg) | dhkl (nm) | D (nm) | Card No. |
|---|---|---|---|---|---|---|---|
| 0.24 | Monoclinic | 35.5983 | 111 | 0.3628 | 2.5304 | 23.16 | 01-070-6828 |
| 1.2 | Monoclinic | 35.4829 | 111 | 0.3965 | 2.5179 | 20.9 | 01-070-6828 |
| 2.4 | Monoclinic | 35.5661 | 111 | 0.4437 | 2.5244 | 18.75 | 01-070-6828 |

absorption peaks of copper were observed. The absorption peaks at (2837 $cm^{-1}$) in the atmosphere's presence of a carbon dioxide molecule. Also, an intense and broad peak was allocated, centered at (3466 $cm^{-1}$), which is considered an expansion of the H-OH bond. And the peak at (1639 $cm^{-1}$) corresponds to the bond C=C.

A spectrum (FTIR) of copper nanoparticles generated using the chemical precipitation process and at various molar concentrations (0.24, 1.2, and 2.4) mM is shown in Figure (3). There were found to be three copper absorption peaks. When a carbon dioxide molecule is present in the atmosphere, the absorption peaks at (2983 $cm^{-1}$). Additionally, a strong and wide peak with a center at (3427 $cm^{-1}$), which is thought to be an expansion of the H-OH bond, was assigned. The vibrational pattern of Cu-O in the $Cu_2O$ phase is linked to the peak centering at (877 $cm^{-1}$) Additionally, the bond C=C is represented by the peak at (1639 $cm^{-1}$). And the modest peak at (2085 $cm^{-1}$) shows that the bond O=C=O has expanded (Moniri et al., 2017; Maisterrena Epstein et al., 2007).

### 3.4 X-ray Diffraction

By using X-ray diffraction, the structural characteristics of the produced nanoparticles were investigated. One of the most crucial methods for the qualitative and quantitative examination of crystalline substances is X-ray diffraction. Bragg's law also described the diffraction principle for these rays. The average crystal size was determined using the Shearer equation, and it was found that the size decreases with increasing molar concentrations. It is demonstrated that these particles have a polycrystalline structure. Copper nanoparticles have a face-centered cubic (FCC) structure, according to diffraction data agrees with the study (?), and the existence of oxide (CuO) suggests that copper nanoparticles have partially oxidized with dissolved oxygen in solution. When exposed to air, oxygen from the surrounding atmosphere quickly develops an oxide coating on the surface of copper nanoparticles. This suggests that, in the context of the current work, de-ionized water as a solvent and alcohol as a catalyst can be used to synthesize copper nanoparticles in an atmospheric environment, at atmospheric pressure, and

**Table 4.** Phases of Copper Nanoparticles

| 2$\theta$ (deg) | Geomtric Crystal System | Phase | Hkl | Card No. |
|---|---|---|---|---|
| 28.6141 | Tetragonal | $Cu_4O_3$ | 112 | 01-071-6397 |
| 32.5228 | Monoclinic | CuO | 110 | 00-041-0254 |
| 35.7431 | Monoclinic | CuO | 111 | 00-041-0254 |
| 36.4813 | Cubic | $Cu_2O$ | 111 | 01-071-3645 |
| 38.7842 | Monoclinic | CuO | 111 | 00-041-0254 |
| 42.3195 | Cubic | $Cu_2O$ | 200 | 01-071-3645 |
| 43.6390 | Cubic | Cu | 111 | 00-001-1242 |
| 46.3775 | Monoclinic | CuO | 112 | 01-070-0828 |
| 47.6224 | Tetragonal | $Cu_4O_3$ | 301 | 01-071-6397 |
| 48.7676 | Tetragonal | $Cu_4O_3$ | 204 | 01-071-6397 |
| 49.8257 | Cubic | Cu | 200 | 00-001-1242 |
| 53.4481 | Monoclinic | CuO | 020 | 00-041-0254 |
| 58.2282 | Monoclinic | CuO | 202 | 00-041-0254 |
| 61.5892 | Cubic | $Cu_2O$ | 220 | 01-071-3645 |
| 66.2697 | Monoclinic | CuO | 022 | 00-041-0254 |
| 67.4149 | Monoclinic | CuO | 113 | 00-041-0254 |
| 68.0373 | Monoclinic | CuO | 220 | 00-041-0254 |
| 72.7925 | Cubic | $Cu_2O$ | 311 | 01-071-3645 |
| 75.1950 | Cubic | Cu | 220 | 00-001-1242 |

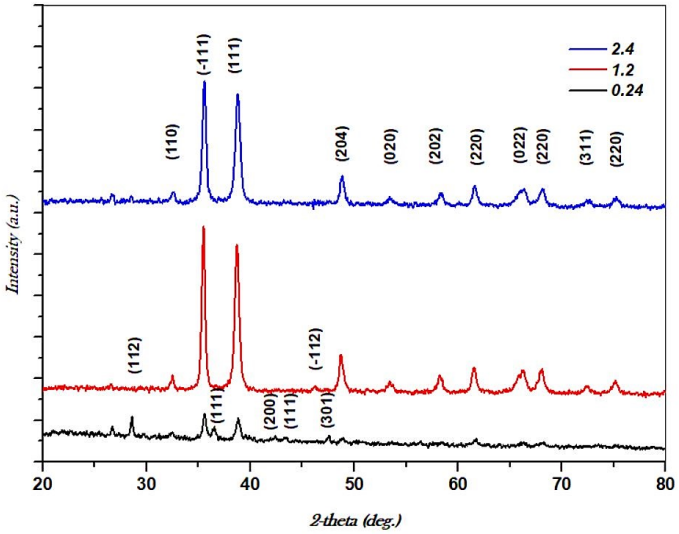


**Figure 4.** X-ray Diffraction of Copper Nanoparticles

ambient temperature. An inert environment is not required to carry out a chemical reaction. Each variable or parameter lowers the process's cost this agrees with (Khalid et al., 2016; Mallik et al., 2020), Figure (4) and Table (3) shows it and the e (4) show for the phases of the copper particles that appeared. All samples contain metal nanoparticles and their oxides, which resulted in the formation of NPs with a core-shell structure. A small displacement of some diffraction peaks may be caused by mechanical stress from various sources, such as impurities, defects, and voids present in the film, as the prevailing trend is

**Table 5.** Average Nanoparticle Size Values

| M (mM) | Average Size (nm) |
|---|---|
| 0.24 | 61.64 |
| 1.2 | 53.84 |
| 2.4 | 49.25 |

also influenced by the deposition technique used. The prevalent trend for the same material varies from sample to sample depending on the deposition technique utilized, and the trends themselves differ. This tendency in crystallization is ascribed to the Drift's survival model for the quickest, The fastest nuclei continue to expand while the growth of other nuclei ceases since it is anticipated that the nucleation process takes more from a direction in the early phases of film growth and then these tendencies begin to compete during their growth. Since the process took place in the air and thus affected the properties of the synthetic sample, the increasing molar concentrations resulted in the formation of efficient scattering centers and may also work to create sniping levels at the grain boundaries that work to snip the charge carriers and freeze them in place. We observe variations in the value of the granular size according to the value concentrations utilized in the preparation when examining the XRD diagnostic results for all of the nanomaterial generated in this study in general and for some Brag angles. It caused the remaining fluid at the substrate's interface to solidify to rearrange the grains and reduce their sizes, but this solidification eventually stopped. X-rays are reflected from different regions of the crystal at different angles as a result of

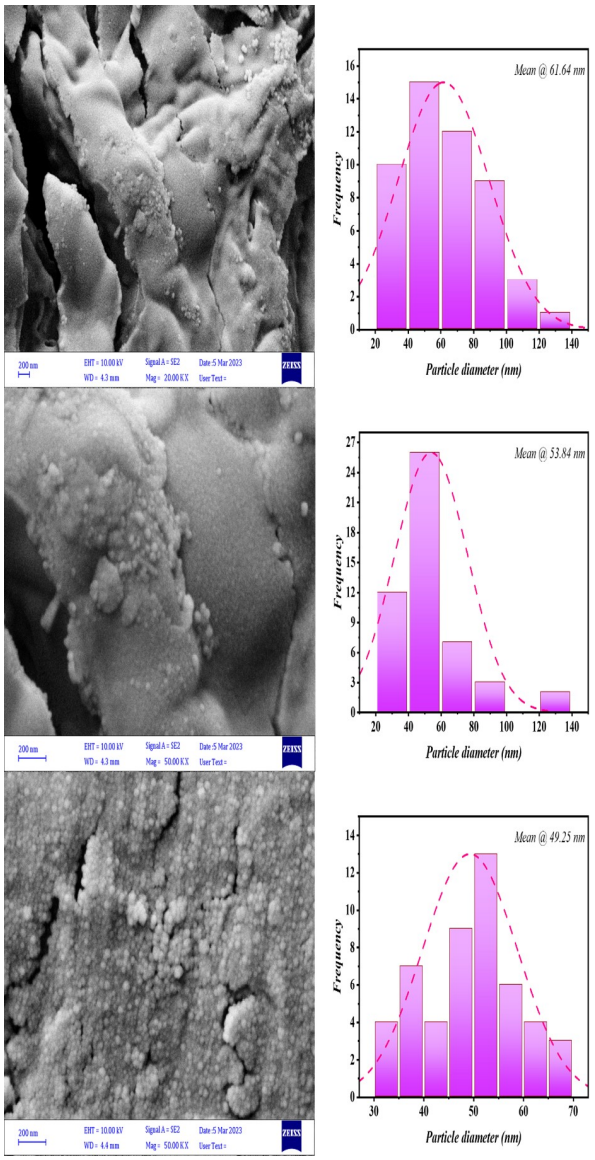


**Figure 5.** FE-SEM of Copper Nanoparticles

the widening of the XRD curve, which may be caused by flaws in the crystal levels and the tiny size of the crystal, In addition, the device being used causes additional widening known as "instrumental broadening" that must be rectified to have the right crystal size. This widening results from the device's usage of subpar optical components like slit width and wavelength width. Additionally, we observe that for a single sample, the interlayer distance (d) is not equal at all Bragg angles, they are not equal at every point in the crystal. This causes each section of the crystal to reflect X-rays at a different angle from the other part, which is consistent with the Ahmad (2010) theory that distinct parts of the crystal reflect light at different angles.

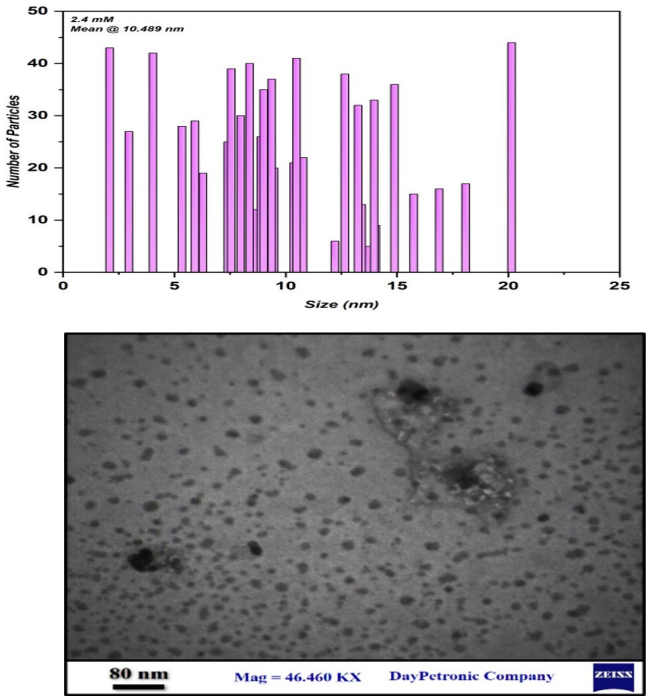


**Figure 6.** TEM of Copper Nanoparticles When 2.4 mM

### 3.5 Filed Emission Scanning Electron Microscopy (FE-SEM) and Transmission Electron Microscopy (TEM) for Nano particles

The minerals' surface morphology was viewed using field emission scanning electron microscopy (FE-SEM). In Figure (5), FE-SEM pictures of the parameters at the applied concentrations are shown. The particles' various forms, irregularities, and unequal particle distribution are demonstrated, Table (4) shows the results for copper nanoparticles . When observed under a (TEM) microscope, they have both a regular and irregular spherical shape and can also be found in clusters. Figure (6) depicts the image of the particle in (TEM) and the average size diameter when concentration (2.4 mM), which is equal to (10.489 nm).

### 3.6 Units, Abbreviations, and Symbols

(CRM) Chemical Reduction Method, (FTIR) Fourier transform infrared, (UV-Vis) Ultraviolet-Visible, (FE-SEM) Filed Emission Scanning Electron Microscope, (TEM) Transmission Electron Microscopy, (FCC) Face Center Cubic, (AAS) Atomic Absorption Spectroscopy, (mM) Mille Mole, (µL) MicroLiter, (µM) Micro Mole, (nm) Nanometer, (SPR) Surface Plasmon Resonance and ($cm^{-1}$) Centimeters$^{-1}$.

## 4. CONCLUSION

This work investigated the ability to synthesize CuNPs by the chemical reduction method The results showed the possibility of obtaining CuNPs using different concentrations through

changing the color of the solution and analyzing the absorption spectrum as a preliminary proof of the nano synthesis of the material, FTIR analysis was conducted and it was found that the effective groups present in the prepared samples are (O-H, C-H, C-O, C=O, and Cu-O-H). As for the structural analysis that was conducted, they included XRD, SEM, and TEM The results obtained roved that the chemical reduction method is an easy and fast method for metal nanosynthesis and it can be a good alternative to other methods. By adjusting the concentration, one can control the size and dispersion of the nanoparticles because the absorption or direct change increases with an increase in concentration. There appears to be more than one phase of copper particles when the concentration count rises because particle size decreases more quickly. In the future, the effect of anti-caking materials that increase surface tension, such as sodium dodecyl sulfate (SDS), or the type of the used solution can be changed instead of using alcohol.

## 5. ACKNOWLEDGMENT

We would like to thank College of Engineering, Tikrit University for to help me with the measurements. Thank you to the Advanced Nano/Micro Optoelectronics Research Center for the structure properties analysis.

## REFERENCES

Ahmad (2010). *The Effect of Thickness on The Optical and Structural Properties of Copper Oxide The Nano- Grain Size*. Thesis, College of Education, Al-Mustansiriya University

Alzahrani, E. (2018). Chitosan Membrane Embedded with ZnO/CuO Nanocomposites for the Photodegradation of Fast Green Dye Under Artificial and Solar Irradiation. *Analytical Chemistry Insights*, **13**; 1177390118763361

Benassai, E., M. Del Bubba, C. Ancillotti, I. Colzi, C. Gonnelli, N. Calisi, M. C. Salvatici, E. Casalone, and S. Ristori (2021). Green and Cost-effective Synthesis of Copper Nanoparticles by Extracts of Non-edible and Waste Plant Materials from Vaccinium Species: Characterization and Antimicrobial Activity. *Materials Science and Engineering: C*, **119**; 111453

Brycki, B., A. Szulc, and M. Babkova (2020). Synthesis of Silver Nanoparticles with Gemini Surfactants as Efficient Capping and Stabilizing Agents. *Applied Sciences*, **11**(1); 154

Duan, H., D. Wang, and Y. Li (2015). Green Chemistry for Nanoparticle Synthesis. *Chemical Society Reviews*, **44**(16); 5778–5792

Gondal, M., T. F. Qahtan, M. A. Dastageer, T. A. Saleh, Y. W. Maganda, and D. H. Anjum (2013). Effects of Oxidizing Medium on the Composition, Morphology and Optical Properties of Copper Oxide Nanoparticles Produced by Pulsed Laser Ablation. *Applied Surface Science*, **286**; 149–155

Harada, M., M. Yamamoto, and M. Sakata (2020). Temperature Dependence on the Size Control of Palladium Nanoparticles by Chemical Reduction in Nonionic Surfactant/ionic Liquid Hybrid Systems. *Journal of Molecular Liquids*, **311**; 113255

Hawthorne, J., C. Musante, S. K. Sinha, and J. C. White (2012). Accumulation and Phytotoxicity of Engineered Nanoparticles To Cucurbita Pepo. *International Journal of Phytoremediation*, **14**(4); 429–442

He, X., D. P. Yang, X. Zhang, M. Liu, Z. Kang, C. Lin, N. Jia, and R. Luque (2019). Waste Eggshell Membrane-templated CuO-ZnO Nanocomposites with Enhanced Adsorption, Catalysis and Antibacterial Properties for Water Purification. *Chemical Engineering Journal*, **369**; 621–633

Huang, J., J. Zhou, J. Zhuang, H. Gao, D. Huang, L. Wang, W. Wu, Q. Li, D. P. Yang, and M. Y. Han (2017). Strong Near-infrared Absorbing and Biocompatible Cus Nanoparticles for Rapid and Efficient Photothermal Ablation of Gram-positive and-negative Bacteria. *ACS Applied Materials & Interfaces*, **9**(42); 36606–36614

Jardón-Maximino, N., M. Pérez Alvarez, G. Cadenas Pliego, L. E. Lugo Uribe, C. Cabello Alvarado, J. M. Mata Padilla, and E. D. Barriga Castro (2021). Synthesis of Copper Nanoparticles Stabilized With Organic Ligands and Their Antimicrobial Properties. *Polymers*, **13**(17); 2846

Jayaramudu, T., K. Varaprasad, R. D. Pyarasani, K. K. Reddy, K. D. Kumar, A. Akbari-Fakhrabadi, R. Mangalaraja, and J. Amalraj (2019). Chitosan Capped Copper Oxide/copper Nanoparticles Encapsulated Microbial Resistant Nanocomposite Films. *International Journal of Biological Macromolecules*, **128**; 499–508

Johnson, M. E., S. Ostroumov, J. Tyson, and B. Xing (2011). Study of the Interactions Between Elodea canadensis and CuO Nanoparticles. *Russian Journal of General Chemistry*, **81**; 2688–2693

Karthik, P. and S. P. Singh (2015). Copper Conductive Inks: Synthesis and Utilization in Flexible Electronics. *RSC Advances*, **5**(79); 63985–64030

Khalid, H., S. Shamaila, N. Zafar, R. Sharif, J. Nazir, M. Rafique, S. Ghani, and H. Saba (2016). Antibacterial Behavior of Laser-ablated Copper Nanoparticles. *Acta Metallurgica Sinica (English Letters)*, **29**; 748–754

Maisterrena Epstein, R., S. Camacho-López, L. Escobar-Alarcón, and M. Camacho-López (2007). Nanosecond Laser Ablation of bulk Al, Bronze, and Cu: Ablation Rate Saturation and Laser-induced Oxidation. *Superficies y vacío*, **20**(3); 1–5

Majumdar, T. D., M. Singh, M. Thapa, M. Dutta, A. Mukherjee, and C. K. Ghosh (2019). Size-dependent Antibacterial Activity of Copper Nanoparticles Against Xanthomonas oryzae pv. oryzae–A Synthetic and Mechanistic Approach. *Colloid and Interface Science Communications*, **32**; 100190

Mallik, M., S. Monia, M. Gupta, A. Ghosh, M. P. Toppo, and H. Roy (2020). Synthesis and Characterization Of Cu2O Nanoparticles. *Journal of Alloys and Compounds*, **829**; 154623

Moniri, S., M. Ghoranneviss, M. R. Hantehzadeh, and M. A. Asadabad (2017). Synthesis and Optical Characterization of Copper Nanoparticles Prepared by Laser Ablation. *Bulletin of Materials Science*, **40**; 37–43

Nagar, N. and V. Devra (2018). Green Synthesis and Charac-

 

terization of Copper Nanoparticles Using Azadirachta Indica Leaves. *Materials Chemistry and Physics*, **213**; 44–51

Nakamura, S., M. Sato, Y. Sato, N. Ando, T. Takayama, M. Fujita, and M. Ishihara (2019). Synthesis and Application of Silver Nanoparticles (Ag NPs) for the Prevention of Infection in Healthcare Workers. *International Journal of Molecular Sciences*, **20**(15); 3620

Patil, S. A., C. H. Ryu, and H. S. Kim (2018). Synthesis and Characterization of Copper Nanoparticles (Cu-Nps) Using Rongalite as Reducing Agent and Photonic Sintering of Cu-Nps Ink for Printed Electronics. *International Journal of Precision Engineering and Manufacturing-Green Technology*, **5**; 239–245

Rashid, S. N., A. S. Jasim, and K. A. Aadimb (2022). Influence of Number of Pulses on Characterization of Nanoparticles of Copper and its Oxides Synthesized by Nd: YAG Laser Ablation Technique and its Antibacterial Activity. *Neuro-Quantology*, **20**(3); 150–159

Seo, Y., J. Hwang, E. Lee, Y. J. Kim, K. Lee, C. Park, Y. Choi, H. Jeon, and J. Choi (2018). Engineering Copper Nanoparticles Synthesized on the Surface of Carbon Nanotubes for Anti-Microbial and Anti-Biofilm Applications. *Nanoscale*, **10**(33); 15529–15544

Vinod, M. and K. Gopchandran (2014). Au, Ag and Au: Ag Colloidal Nanoparticles Synthesized by Pulsed Laser Ablation as SERS Substrates. *Progress in Natural Science: Materials International*, **24**(6); 569–578

Wu, R., Z. Ma, Z. Gu, and Y. Yang (2010). Preparation and Characterization of CuO Nanoparticles with Different Morphology Through a Simple Quick-precipitation Method in DMAC–water Mixed Solvent. *Journal of Alloys and Compounds*, **504**(1); 45–49

Xu, J., K. Yu, J. Wu, D. Shang, L. Li, and Z. Zhu (2009). Synthesis, Field Emission and Humidity Sensing Characteristics of Honeycomb-like CuO. *Journal of Physics D: Applied Physics*, **42**(7); 075417

Zahoor, M., N. Nazir, M. Iftikhar, S. Naz, I. Zekker, J. Burlakovs, F. Uddin, A. W. Kamran, A. Kallistova, and N. Pimenov (2021). A Review on Silver Nanoparticles: Classification, Various Methods of Synthesis, and Their Potential Roles in Biomedical Applications and Water Treatment. *Water*, **13**(16); 2216

Zhi Ang, J., C. Jiang Tao, W. Jun, Z. Ren Fu, Y. De, Z. Fei, and Y. Peng Xun (2009). CuO Nanosheets Synthesized by Hydrothermal Process. *Chinese Physics Letters*, **26**(8); 086202

Zhou, K., R. Wang, B. Xu, and Y. Li (2006). Synthesis, Characterization and Catalytic Properties of CuO Nanocrystals with Various Shapes. *Nanotechnology*, **17**(15); 3939

 